



Mechanistic insights and therapeutic implications of novel pyrazoline derivatives on antioxidant and enzymatic inhibitory activities

I. Selatnia^{a,*}, O.M.A. Khamaysa^a, A.G. Soliman^b, R. Bourzami^c, A. Sid^a, H. Lgaz^{d,*}, K. Mokhnache^e, Awad A. Alrashdi^f, C. Bensouici^g

^a Laboratory of Analytical Sciences, Materials and Environmental (LSAME), Larbi Ben M'Hidi University, Oum El B ouaghi, 04000, Algeria

^b Agricultural Biochemistry Department, Faculty of Agriculture, Ain Shams University, Shoubra El-Kheima, Cairo, Egypt

^c Research unit on emerging materials, university Ferhat Abbas Setif 1 Setif, Algeria

^d Innovative Durable Building and Infrastructure Research Center, Center for Creative Convergence Education, Hanyang University ERICA, 55 Hanyangdaehak-ro, Sangrok-gu, Ansan-si, Gyeonggi-do 15588, South Korea

^e Laboratory of Applied Biochemistry, Ferhat Abbas University of Setif, 19000, Algeria

^f Chemistry Department, Umm Al-Qura University, Al-Qunfudah University College, Saudi Arabia

^g National Research Centre for Biotechnology, Constantine 25000, Algeria

ARTICLE INFO

Keywords:

Pyrazoline derivative
DFT
AChE
ADMET
PDB

ABSTRACT

One of the major features of medicinal chemistry, is the synthesis of novel compounds, and the assessment of their biological activities for potential therapeutic applications. As a contribution to this filed of interest, the present work examines the effects of newly synthesized pyrazoline derivatives. To this end, four pyrazoline derivatives were synthesized and evaluated for their antioxidant activities and enzymatic inhibitory in vitro against acetylcholinesterase (AChE) and tyrosinase. All the synthesized compounds **2a–2d** all displayed a moderate to potent antioxidant activity. For the enzymatic inhibitory activity, compound **2a** exerted the most potent acetylcholinesterase inhibition with an IC_{50} value of ($IC_{50} = 3.93 \pm 0.52 \mu M$) which is twice greater than the standard drug, Galantamine ($IC_{50} = 6.27 \pm 1.15 \mu M$), whereas, compound **2a** was determined as the best inhibitor among the synthesized compounds for the tyrosinase enzyme with an IC_{50} value of ($32.65 \pm 2.30 \mu M$). Density Functional Theory (DFT) calculations were performed to determine the compound's properties, and molecular docking studies were conducted to discuss potential interactions between the most active compound (**2a**) and active sites of proteins AChE (PDB: 1ACL) and tyrosinase (PDB: 2Y9X). Based on in silico predictions of Absorption, Distribution, Metabolism, Excretion and Toxicity (ADMET) and pharmacokinetic parameters, it is suggested that these compounds could potentially exhibit favorable oral bioavailability. The paper offers promising insights into the therapeutic potential of these pyrazoline derivatives, particularly compound **2a**. It encourages further investigation into the practical application of these findings, possibly leading to new therapeutic avenues in the treatment of diseases associated with acetylcholinesterase and tyrosinase.

1. Introduction

Reactive oxygen species (ROS) — including superoxide anion radical ($O_2^{\cdot-}$), hydroxyl radical (OH^{\cdot}), alkoxyl radical (RO^{\cdot}), and lipid peroxidation — are involved in various processes essential to human body function, such as signal transduction and the biochemical synthesis of significant cellular compounds [1]. However, their excessive presence can create an imbalance between the free radicals and their neutralization, potentially leading to numerous types of biological damage that can cause diseases such as Alzheimer's, inflammatory disorders, cancer,

and neurodegenerative diseases [2]. Therefore, to prevent the harm caused by free radicals and ROS, the utilization of antioxidants, whether synthetic or natural, is essential [3]. The field of drug discovery stands at the forefront of medical science, continuously striving to uncover novel strategies for combating diseases that afflict humanity. Enzymes are attractive targets for drug therapy because of their essential roles in biological processes involved in diseases' pathophysiology [4]. The research conducted by Hopkins and Groom [5] revealed that 47 % of all marketed small-molecule drugs inhibit enzymes as their molecular target. Because of this susceptibility to inhibition by small-molecule

* Corresponding authors.

E-mail addresses: selatnia.ilhem@univ-oeb.dz (I. Selatnia), hlgaz@hanyang.ac.kr (H. Lgaz).

<https://doi.org/10.1016/j.molstruc.2023.136761>

Received 29 June 2023; Received in revised form 27 September 2023; Accepted 2 October 2023

Available online 4 October 2023

0022-2860/© 2023 Elsevier B.V. All rights reserved.

drugs, enzymes are commonly the target of new drug discovery and design efforts at major pharmaceutical and biotechnology companies today [6]. Alzheimer's disease (AD) is a complex and progressive neurodegenerative disorder with a lack of cognition in new learning and holding information in mind that is characterized by the progressive and irreversible loss of neurons located in specific brain areas which pose a significant global health challenge [7]. With the aging population on the rise, the prevalence of AD has reached unprecedented levels, where the number is expected to reach 152 million by 2050 [8], making it imperative to comprehend its intricate mechanisms and explore avenues for effective intervention. It is well known that acetylcholinesterase is the key enzyme in acetylcholine degradation into its inactive form, leading to reduced communication and signaling between nerve cells [9]. Accordingly, the use of acetylcholinesterase (AChE) inhibitors such as donepezil, rivastigmine, and galantamine is one of the most well-known treatments for Alzheimer's disease, via the blockage of the acetylcholinesterase responsible for destroying acetylcholine which causes an increase in the concentration of the neurotransmitter acetylcholine in the brain, and this, in turn, improves memory [7]. Skin hyperpigmentation, characterized by the excessive production and accumulation of melanin pigment within the skin, poses a significant cosmetic concern and often results from various factors, including UV radiation exposure, hormonal imbalances, and skin aging [10,11]. Tyrosinase, a copper-containing metalloenzyme plays a pivotal role in the melanogenesis process that takes place in the epidermis by catalyzing the hydroxylation of L-tyrosine to L-DOPA, and the oxidation of L-DOPA to dopaquinone reactions [12,13]. These reactions are essential for the production of melanin which exerts skin protective functions against harmful ultraviolet radiation and prevention of cancer development [14]. Thus, inhibiting tyrosinase becomes imperative to mitigate the adverse consequences stemming from an excess of melanin production [15] (Fig. 1).

Nitrogen-containing heterocyclic compounds have recently attracted much attention in biological, medicinal chemistry, and drug design research [16]. They are found in a vast variety of natural compounds,

such as nicotine, vitamin B1, and Penicillin, and their versatility is due to their unique pharmaceutical properties [17,18]. Among the various classes of N-heterocycle compounds, pyrazoline derivatives are one of the most biologically active molecules [19,20], which are present in several drugs and have demonstrated a range of biological activities such as antibacterial [21–23], antifungal [24], antidepressant [25], anticancer [26], Anticholinesterase [27,28], and anti-inflammatory properties [29]. They also exhibit promising potential as anticancer agents due to their ability to inhibit enzymes that facilitate cell division [30,31]. Recently, pyrazoline derivatives have gained attention as potential antioxidant agents due to their capability to prevent oxidative damage by quenching free radicals [32,33].

In silico approaches have emerged as powerful tools in biological fields, enabling researchers to analyze and predict the behavior of complex biological systems using computer algorithms and simulations, offering a cost-effective and time-efficient solution [34]. Additionally, molecular docking is a computational method used to predict the binding affinity of a small molecule ligand to a protein target, potentially useful for drug discovery [35,36]. Given the pharmacological importance of pyrazoline derivatives, this study aimed to evaluate the antioxidant and inhibitory activity against acetylcholinesterase (AChE) and tyrosinase of four pyrazoline derivatives (Fig. 2). DFT calculations of the target compounds at the B3LYB/6–31 G (d,p) level were performed to investigate their reactivity and biological significance. The drug-likeness and ADMET properties of the title compounds were also examined and discussed. Moreover, a molecular docking analysis was conducted to investigate the interactions between the compounds and proteins.

2. Experimental

2.1. Material and methods

In the present study, all the chemicals and reagents were purchased from Sigma Aldrich or Merck and used as received without further purification. 2-Acetonaphthone (99 %), p-Tolualdehyde (97 %), 4-Chlorobenzaldehyde (97 %), 4-Isopropylbenzaldehyde (98 %), 2,4-Dihydroxybenzaldehyde (98 %), Hydrazine monohydrate (98 %), ethanol (99.5 %), NaOH (reagent grade, ≥ 98 %, pellets (anhydrous)), DMSO (ACS reagent, ≥ 99.9 %), HCl (ACS reagent, 37 %), Ethyl acetate (99.8 %), Formic acid (reagent grade, ≥ 95 %), DPPH (2,2-diphenyl-1-picrylhydrazyl), ABTS (2,2-Azinobis(3-Ethylbenzthiazolin-6-Sulfonic Acid 98 %), Copper (II) chloride (powder, 99 %), Ammonium acetate (reagent grade, ≥ 98 %), Potassium persulfate (ACS reagent, ≥ 99.0 %), neocuproine (≥ 98.0 %), a-tocopherol ≥ 95.5 %, electric eel AChE (Type-VI-S, EC 3.1.1.7, 425.84 U/mg), 5,5'-Dithiobis(2-nitrobenzoic acid) (DTNB) (98 %), Acetylthiocholine iodide (≥ 99.0 %), galantamine, Nitro Blue Tetrazolium (NBT), 3,4-dihydroxy-L-phenylalanine (LDOPA) (≥ 98.0 %), Kojic acid, tyrosinase from mushroom (EC 232–653–4, 250 KU, ≥ 1000 U/mg solid).

All reactions and Purity of the synthesized compounds were checked by Analytical thin layer chromatography (TLC) carried out on percolated TLC plates (silica gel 60F254, Merck) and the spots were visualized by UV light and stained with either phosphomolybdic acid or *p*-anisaldehyde. Melting points of the compounds were determined on a capillary melting point apparatus and are uncorrected. ^1H and ^{13}C NMR spectra are recorded on a Bruker spectrometer respectively at 400 and at 100 MHz in CDCl_3 and DMSO (internal standard TMS, $\delta = 0.0$ ppm) at room temperature. The following abbreviations were used to explain the multiplicities: *s* = singlet, *dd* = doublet, *m* = multiplet. Infrared spectra were recorded in KBr on Perkin-Elmer AC-1 spectrophotometer. Microanalyses were performed on Carlo Erba EA-1108 element analyzer and were within the ± 0.4 % of the theoretical values. Column chromatography was performed on silica gel (Merck, 60–120 mesh).

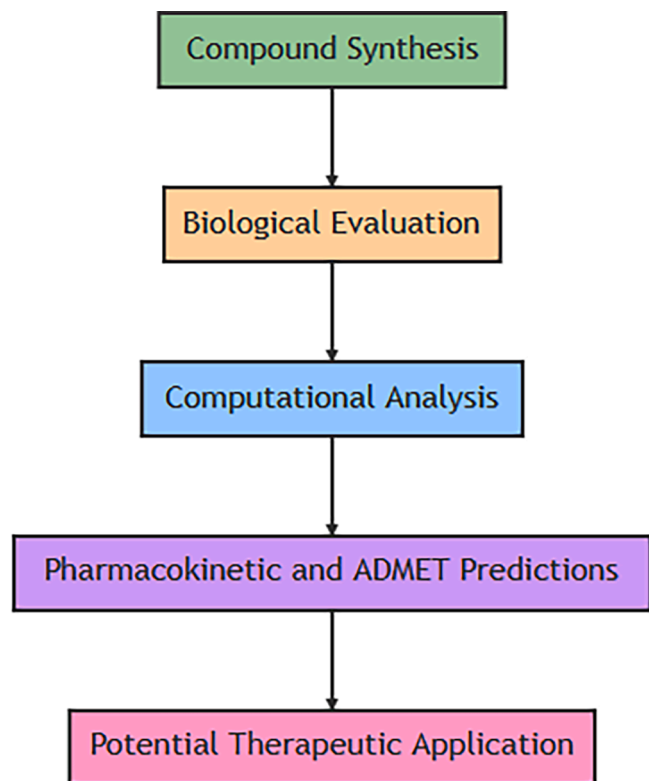


Fig. 1. Visual representation of the study's design strategy.

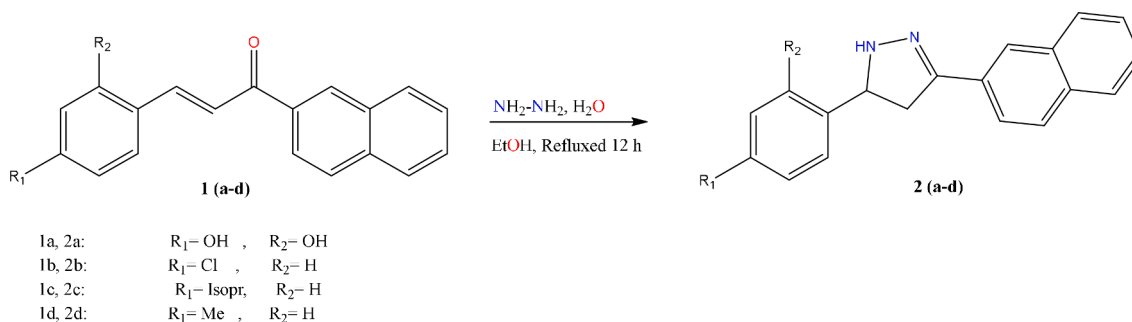


Fig. 2. Synthesis pathway of the target compounds.

2.2. Synthesis

The synthesis of pyrazolines derivatives was carried out in two steps. Our synthetic route begins by the preparation of the (*P*- and *o*, *p*-substituted benzylidene)-acrylonaphthones (**1a–1d**) by condensation of substituted benzaldehydes and 2-Acetonaphthone in ethanol and 10 % sodium hydroxide using an ice bath, according to the reported procedure [37]. Then the obtained chalcones (**1a–1d**) (0.001 mol) was mixed with 8 ml of hydrazine hydrate in 20 ml of EtOH, which offers the appropriate 2-pyrazolines derivatives (**2a–2d**) after refluxed for 12 h. The obtained spectroscopic results and physical properties are in full agreement with literature reports [38], the resultant data as shown in Table 1.

• 3-(naphthalen-2-yl) –5- (2,4-dihydroxyphenyl)–2-pyrazoline (2a)

- ✓ UV (nm): 218 (ϵ : 2.848);
- ✓ FT-IR (KBr, cm^{-1}): 3178 (N–H), 2930.45 (C–H), 1630.04 (C=N), 1275.24– 1076.56 (C–N);
- ✓ ^1H NMR (400 MHz, DMSO) δ : 3.29 (dd, $J = 18.4, 4.8$ Hz, 1H), 3.81 (dd, $J = 18.4, 11.9$ Hz, 1H), 5.51 (dd, $J = 11.9, 4.8, 1.0$ Hz, 1H), 7.27–7.47 (m, 5H Ar), 7.48–7.51 (m, 3H Ar), 7.58–7.62 (m, 2H Ar), 10.08 (2H, s, OH).
- ✓ ^{13}C NMR (100 MHz, DMSO) δ : 41.95 (CH₂), 58.8, 125.6, 126.6, 127.05, 128.8 (10 CH-Ar), 130.6, 131.0, 138.9, 147.7 (6 C-Ar), 154.7 (C=N).
- ✓ Anal. calcd. for C₁₉H₂₂N₂O₂: C, 74.00; H, 6.54; N, 9.08. Found: C, 73.96; H, 6.50; N, 9.04 %.

• 3-(naphthalen-2-yl) –5- (4-chlorophenyl)–2-pyrazoline (2b)

- ✓ UV (nm): 227 (ϵ : 3.957);
- ✓ FT-IR (KBr, cm^{-1}): 3288.04 (N–H), 2925.48 (C–H), 1635 (C=N), 1290.14– 1089.58 (C–N), 777.172 (C–Cl);
- ✓ ^1H NMR (400 MHz, CDCl₃) δ : 3.23 (dd, $J = 18.4, 4.8$ Hz, 1H), 3.70 (dd, $J = 18.4, 11.9$ Hz, 1H), 4.96 (ddd, $J = 11.9, 4.8, 1.0$ Hz, 1H), 7.33–7.44 (m, 5H Ar), 7.52–7.82 (m, 4H Ar), 7.84–7.87 (m, 2H Ar).
- ✓ ^{13}C NMR (100 MHz, CDCl₃) δ : 41.98 (CH₂), 58.89 (CHX), 125.71, 126.75, 127.25, 128.91 (11 CH-Ar), 131.42, 131.72, 139.14, 148.1 (5 C-Ar), 155.25 (C=N).
- ✓ Anal. calcd. for C₁₉H₁₉ClN₂: C, 73.42; H, 6.16; N, 9.01. Found: C, 73.38; H, 6.12; N, 8.98 %.

• 3-(naphthalen-2-yl) –5- (4-isopropylphenyl)–2-pyrazoline (2c)

- ✓ UV (nm): 223 (ϵ : 3.858);
- ✓ FT-IR (KBr, cm^{-1}): 3187.06 (N–H), 2928.60 (C–H), 1633.04 (C=N), 1280.24–1079.58 (C–N);
- ✓ ^1H NMR (400 MHz, CDCl₃) δ : 1.23 (d, $J = 6.9$ Hz, 6H), 2.90 (sept, $J = 6.9$ Hz, 1H), 3.32 (dd, $J = 4.6, 17.7$ Hz, 1H), 3.82 (dd, $J = 11.8, 17.7$ Hz, 1H), 5.52 (dd, $J = 4.6, 17.7$ Hz, 1H), 7.32–7.42 (m, 5H Ar), 7.54–7.79 (m, 4H Ar), 7.85–7.88 (m, 2H Ar).

- ✓ ^{13}C NMR (100 MHz, CDCl₃) δ : 23.90, 23.92, 33.77 (CH(CH₃)₂), 42.60 (CH₂), 58.80 (CHX), 125.62, 126.69, 127.08, 128.81 (11 CH-Ar), 130.62, 130.97, 137.94, 148.59 (5C-Ar), 155.25 (C=N).
 - ✓ Anal. calcd. For C₂₂H₂₆N₂: C, 82.97; H, 8.23; N, 8.80. Found: C, 82.93; H, 8.20; N, 8.76 %.
- ### • 3-(naphthalen-2-yl) –5- (4-methylphenyl)–2-pyrazoline (2d)
- ✓ UV (nm): 238 (ϵ : 3.135);
 - ✓ FT-IR (KBr, cm^{-1}): 3345.89 (N–H), 2921.63 (C–H), 1637.27 (C=N), 1384.64 (C–N);
 - ✓ ^1H NMR (400 MHz, CDCl₃) δ : 1.20 (s, 3H), 3.27 (dd, $J = 18.3, 4.8$ Hz, 1H), 3.82 (dd, $J = 18.3, 11.8$ Hz, 1H), 5.53 (dd, $J = 11.8, 4.8, 1.0$ Hz, 1H), 7.30–7.45 (m, 5H Ar), 7.467.50 (m, 4H Ar), 7.68–7.72 (m, 2HAr);
 - ✓ ^{13}C NMR (100 MHz, CDCl₃) δ : 23.85 (CH₃), 42.40 (CH₂), 57.70, 125.60, 126.59, 127.02, 128.80 (11 CH-Ar), 130.59, 130.95, 137.86, 148.48 (5 C-Ar), 155.8 (C=N).
 - ✓ Anal. calcd. for C₂₀H₂₂N₂: C, 82.72; H, 7.64; N, 9.65. Found: C, 82.68; H, 7.60; N, 9.61 %.

2.3. Computational calculations

The synthesized pyrazoline compounds were optimized in a vacuum, by the B3LYP method [39] with 6–31 G (d,p) level of theory of GAUSSIAN 09 package. Koopman theorem [40] and Pearson and Parr [41,42] were used to calculate several theoretical descriptors in order to study the chemical behavior of the synthesized compounds.

2.4. Bioassays

2.4.1. Determination of antioxidant activity

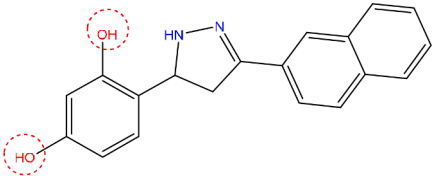
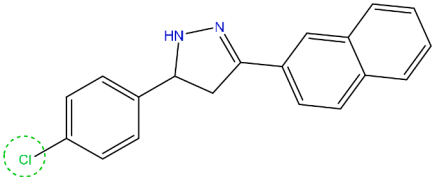
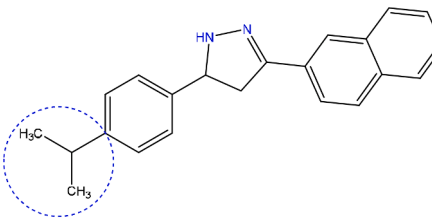
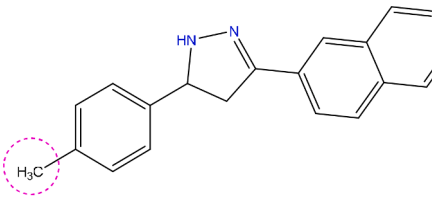
The antioxidant activity of the synthesized pyrazolines derivatives was evaluated using four complementary assays namely: Free-radical scavenging activity by DPPH assay [43], Cupric reducing antioxidant capacity assay by neocuproine-Cu⁺ complexation (CUPRAC) [44], ABTS cation radical decolorization [45], as well as Superoxide assay [46], which performed using a 96 well microplate reader (Spectra Max, Molecular Devices, California, USA). DMSO was utilized as a control, whereas α -Tocopherol was utilized as antioxidant standards. The results obtained were reported as IC₅₀ ($\mu\text{g ml}^{-1}$), representing the concentration at which 50 % inhibition occurred, except for the CUPRAC results, which were reported as A_{0.5} ($\mu\text{g ml}^{-1}$), representing the concentration indicating 0.50 absorbance intensity

2.4.2. Determination of acetylcholinesterase (AChE) inhibitory activity

The Ellman spectrophotometric method with slight modification was utilized to measure the inhibitory activity of Acetylcholinesterase (AChE) [47]. The absorbance was measured at 412 nm. Galantamine was taken as a positive control. The percentage inhibition (%) was calculated as follows:

$$\text{inhibition (\%)} = \frac{C - S}{C} \times 100 \quad (1)$$

Table 1
Chemical structures of the synthesized pyrazolines.

Chemical structure of the target compounds	Formula	Color	Mol wt. (g/mol)	Yield (%)	MP (°C)
 <p>3-(naphthalen-2-yl)-5-(2,4-dihydroxyphenyl)-2-pyrazoline (2a)</p>	C ₁₉ H ₁₆ N ₂ O ₂	Brown cristal	304	62	39–40
 <p>3-(naphthalen-2-yl)-5-(4-chlorophenyl)-2-pyrazoline (2b)</p>	C ₁₉ H ₁₅ ClN ₂	White cristal	306.5	82	156–157
 <p>3-(naphthalen-2-yl)-5-(4-isopropylphenyl)-2-pyrazoline (2c)</p>	C ₂₂ H ₂₂ N ₂	White cristal	314	70	95–96
 <p>3-(naphthalen-2-yl)-5-(4-methylphenyl)-2-pyrazoline (2d)</p>	C ₂₀ H ₁₈ N ₂	White cristal	286	57	101–102

Where: C is the activity of enzyme without test sample and S is the activity of enzyme with test sample.

2.4.3. Determination of tyrosinase inhibitory activity

Tyrosinase inhibition activity was measured according to the method established by Chan et al. [48]. L-DOPA was used as substrate and kojic acid was used as standard inhibitors of tyrosinase. The percentage tyrosinase inhibition (%) was calculated according the following formula:

$$\text{inhibition (\%)} = \frac{\text{Absorbance control} - \text{Absorbance sample}}{\text{Absorbance control}} \times 100 \quad (2)$$

2.4.4. Statistical analysis

All bioassays were conducted three times. The data were expressed as mean \pm standard error (SEM). Statistical significance between means was determined using Student's *t*-test, and values of $p < 0.05$ were considered significant.

2.5. Target prediction

Potential target prediction was estimated for all 4 tested compound using Swiss Target prediction web server (<http://www.swisstargetprediction.ch/>) for homo sapiens receptor targets by searching using SMILES

code for all test set one by one

2.6. Molecular docking

The pyrazoline derivatives structures **2a–2d** were built and energy-minimized with Density Functional Theory (DFT) using functional Becke-3-Lee Yang Parr (B3LYP) method and 6–31 G (d, p) basis set. The crystallographic structures of acetylcholinesterase (PDB ID: 1ACJ) [49] and tyrosinase (PDB ID: 2Y9X) [50] were obtained from the RSCB data bank (<https://www.rcsb.org>). Molecular docking analyzes of the selected pyrazoline (**2a**), Kojic acid and Galantamine at the target protein binding site was performed with AutoDock 4 software. Water molecules were removed, then polar hydrogen atoms and the Kollmann charges were added to the receptors. The grid box is of dimension $20 \times 20 \times 20$ points with a radius of 0.375 Å with coordinates x: –11.174, y: –30.719, and z: –44.43 for anti-tyrosinase activity. For anticholinesterase activity it is of $20 \times 20 \times 20$ points with a radius of 0.500 Å with coordinates x: 2.332, y: 65.332, and z: 70.915. The conformations with the lowest binding energy were selected and the interactions were analyzed using Discovery Studio Visualizer 19.1.

2.7. Drug likeness properties and ADMET analysis

Absorption, Distribution, Metabolism, Excretion, and Toxicity (ADMET), and it is a set of properties used to predict the pharmacokinetics and pharmacodynamics of a compound. All synthesized pyrazoline derivatives were screened by estimating their ADMET properties using SWISS ADME (www.swissadme.ch) and pkCSM (<http://biosig.unimelb.edu.au/pkcsm/>) servers.

3. Results and discussion

3.1. Synthesis

The synthesis of pyrazoline derivatives **2a–2d**, as illustrated in Fig. 2, was monitored using the TLC method. Initially, the Claisen–Schmidt condensation of substituted benzaldehydes and 2-Acetonaphthone in the presence of NaOH in EtOH resulted in (P- and o, p-substituted benzylidene)-acrylonaphthones (**1a–1d**). Subsequently, the intermolecular cyclization of compounds (**1a–1d**) with hydrazine hydrate under reflux yielded the corresponding 2-pyrazoline derivatives (**2a–2d**) in good to excellent yields (65–86 %). The structural elucidation of the obtained compounds was confirmed by IR and NMR spectroscopy.

The UV–vis spectra of the pyrazolines derivatives in ethanol showed absorption bands at (320–330 nm), (335–340 nm), and (405–410 nm) assignable respectively to $n-\pi^*$, $\pi-\pi^*$ and $n-\sigma^*$ transitions. Substituted pyrazolines have strong fluorescence in different solvents. They also give excellent fluorescence properties in solid state because the conjugation system contains two nitrogen atoms and one carbon atom while the other carbon atoms are sp^3 hybrids. Their spectra showed a band for

the C–N group at (1275–1284 cm^{-1}) and a band (1630–1637 cm^{-1}) for C=N. In the 1H NMR spectra of synthesized compounds, the three hydrogen atoms attached to the heterocyclic ring gave an ABX spin system in which the measured chemical shift and coupling constant values prove the 2-pyrazoline structure. In the ^{13}C NMR spectra the carbon atoms chemical shift values of the heterocyclic ring C=N (145.8–155.25 ppm), C-4 (41.95–42.40 ppm) and C-5 (57.70–58.89 ppm) corroborate the 2-pyrazoline structures determined by 1H NMR spectroscopic measurements.

3.2. Quantum chemical calculations

3.2.1. Geometry optimization

The geometry optimization of the synthesized molecules was performed in vacuum, using Density Functional Theory (DFT) with the B3LYP method and a 6–31 G (d, p) basis set. Fig. 3 presents the most stable conformations of the pyrazoline molecules. The top panel displays top views, while the bottom panel shows side views. All the molecules maintain planar conformations, except for the carbon atoms with sp^3 hybridization, which retain tetrahedral geometry. Furthermore, planar geometry provides an external steric environment, a feature potentially useful for electron exchange with the external medium

3.2.2. Mapping electrostatic potential (MEP)

The surfaces of total electron density, determined by the electrostatic potentials of ligands **2a**, **2b**, **2c**, and **2d**, are shown in Fig. 4. The surfaces are notably similar, with all molecules exhibiting weak negative potentials in the most geometric zones, as no red area is observed. Significant negative potentials, indicated by yellow color, are located around aromatic cycles and oxygen atoms—sites that can attract nucleophilic substances. On the other hand, positive potentials, indicated by a blue color area, are situated around hydrogen atoms, designating the electrophilic area around the molecular structures. The heterogeneity of these four potential molecular distributions results in different dipole moment values: 4.429, 2.908, 1.153, and 1.077 Debye for **2a**, **2b**, **2c**, and **2d**, respectively. The dipolar moment values for **2a** and **2b** are higher than those for **2c** and **2d**, due to high negative partial charges centered on chlorine and oxygen atoms.

3.2.3. Frontier molecular orbitals (FMOs)

Molecular orbitals and their energies provide essential insights into electronic properties and chemical reactions [51]. The E_{HOMO} is related to the electron-donating ability and ionization potential, while the E_{LUMO} relates to electron-accepting ability and electron affinity. Fig. 5 presents the calculated frontier orbitals of the synthesized pyrazoline. Electrons of the HOMO are predominantly localized on the pyrazoline ring and phenyl ring moieties, while those of the LUMO are primarily found on the naphthalene moiety. Table 2 summarizes E_{HOMO} , E_{LUMO} , energy gap ΔE , and other key physicochemical parameters: ionization potential (I), global electrophilicity (ω), global softness (σ), chemical

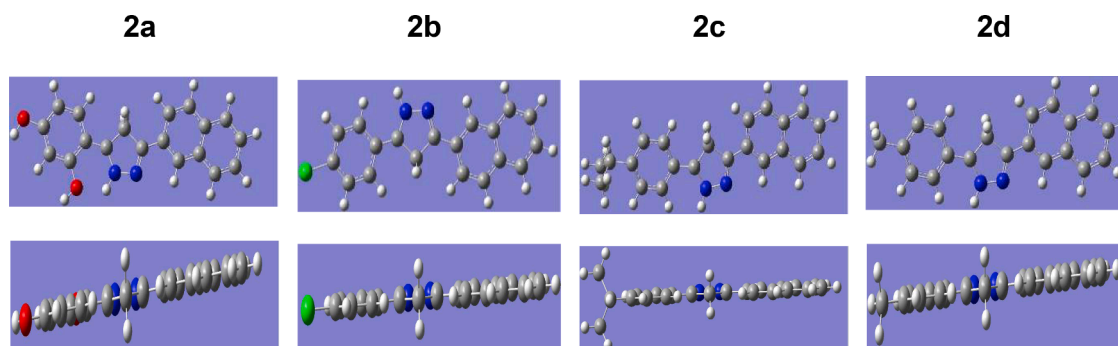


Fig. 3. Optimized structures of the target compounds.

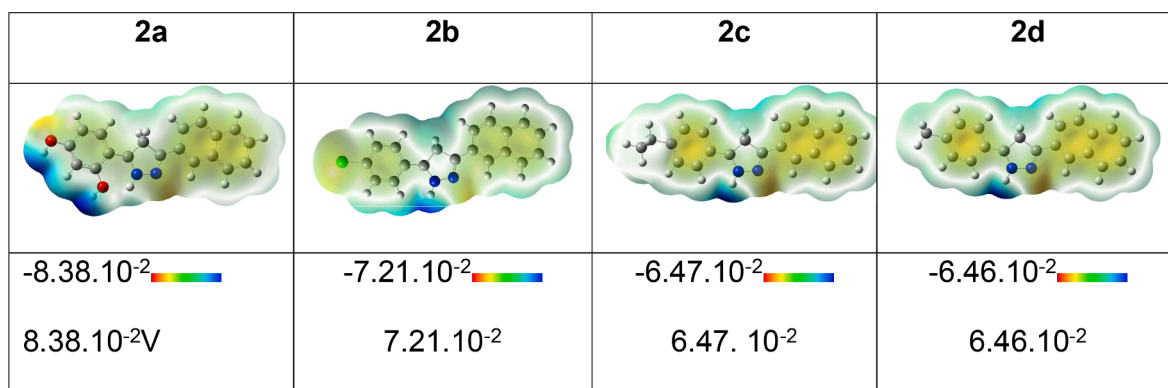


Fig. 4. Mapping electrostatic potential.

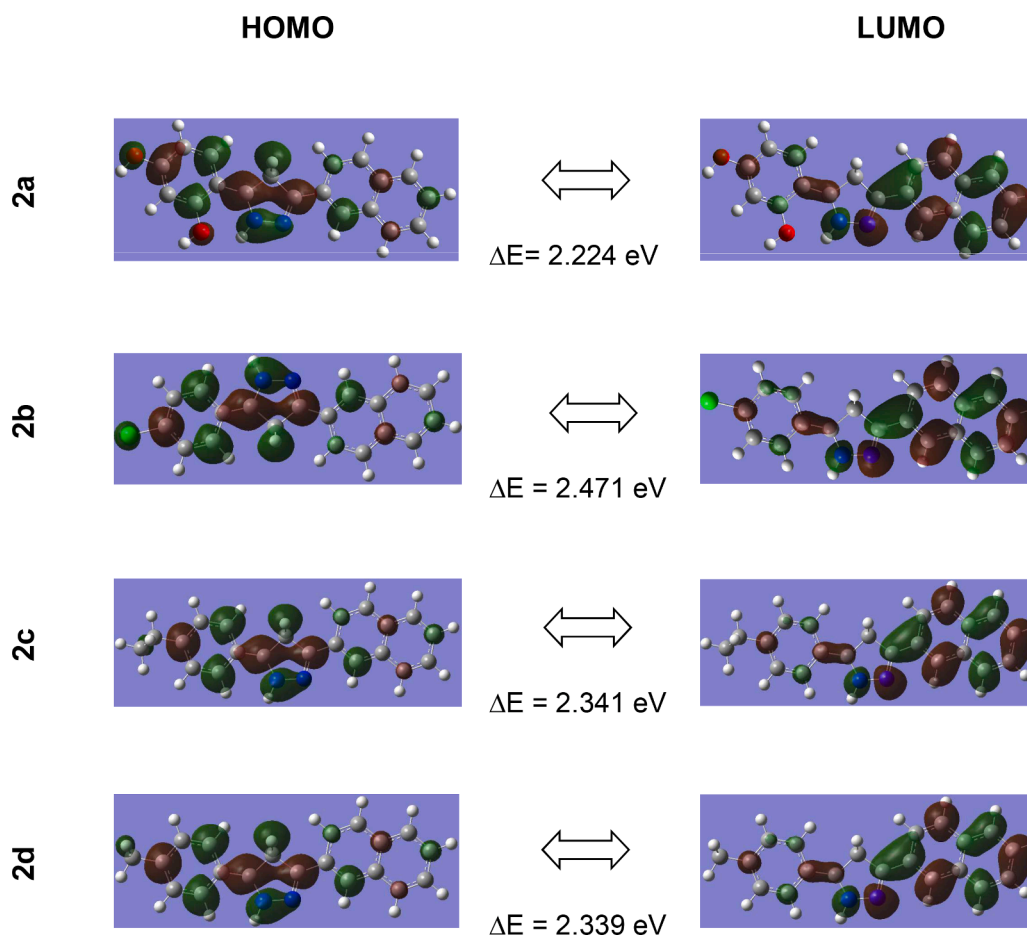


Fig. 5. Calculated frontier molecular orbitals.

potential (μ), electronegativity (χ), global hardness (η), and electron affinity (A). The energy gap is defined as the energy difference between E_{LUMO} and E_{HOMO} . Fig. 6 illustrates the comparison between the frontier levels and their corresponding energy values for all the molecules, with calculated energy values of 2.224, 2.339, 2.341, and 2.471 for **2a**, **2b**, **2c**, and **2d**, respectively. These relatively low energy values suggest that the synthesized molecules can exchange electrons with the external medium. The low values of E_{LUMO} affirm the electron-accepting ability, which may explain the good antioxidant performance of these molecules. Additionally, the high values of global hardness (η) and the low softness value (σ) denote the ability to exchange electrons with other species [52].

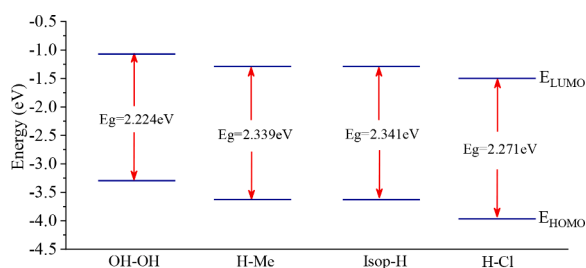
3.3. Evaluation of antioxidant activity

All the synthesized target compounds were evaluated for their antioxidant activity, and the results are displayed in Table 3. DPPH activity results demonstrated that compounds **2a** and **2b** exhibited significant activity, presenting a minimum IC_{50} value of $48.21 \pm 2.03 \mu\text{M}$ and $56.32 \pm 1.62 \mu\text{M}$, respectively. These results were compared to the standard, α -Tocopherol, with an IC_{50} of $13.02 \pm 5.17 \mu\text{M}$. Compounds **2c** and **2d** demonstrated moderate activity in comparison to the standard. Furthermore, all tested compounds displayed potent superoxide radical scavenging activity, where compounds **2a** ($9.53 \pm 1.52 \mu\text{M}$) and **2b** ($11.33 \pm 1.01 \mu\text{M}$) demonstrated superior antioxidant activity

Table 2

Calculated HOMO and LUMO energies and some related physicochemical parameters.

Compounds	2a	2b	2c	2d
<i>Electronic band energies</i>				
E_{HOMO} (eV)	-3.295	-3.968	-3.630	-3.628
E_{LUMO} (eV)	-1.071	-1.497	-1.289	-1.289
Energy gap (Δ) (eV)	2.224	2.471	2.341	2.339
<i>Electrochemical parameters</i>				
Dipolar moment (Debye)	4.425	2.908	1.077	1.153
Ionization potential (I)	3.295	3.968	3.630	3.628
Global electrophilicity (ω)	2.224	3.008	2.340	2.338
Global softness (σ)	0.899	0.809	0.854	0.855
Chemical potential (μ)	-2.183	-2.732	-2.459	-2.458
Electronegativity (χ)	2.183	2.732	2.459	2.458
Global hardness (η)	1.112	1.235	1.170	1.169
Electron affinity (A)	1.071	1.497	1.289	1.289

**Fig. 6.** Comparison of the frontier levels and their related energy values.**Table 3**

Antioxidant activity of the synthesized pyrazoline by the DPPH, CUPRAC, ABTS and superoxide anion radical assays.^a

Compounds	DPPH assay IC ₅₀ (μM) ^a	CUPRAC assay A _{0.50} (μM) ^a	ABTS assay IC ₅₀ (μM) ^a	Superoxide anion radical assay IC ₅₀ (μM) ^a
2a	48.21 ± 2.03	23.81 ± 0.25	10.48 ± 0.14	9.53 ± 1.52
2b	56.32 ± 1.62	35.21 ± 0.91	19.25 ± 0.72	11.33 ± 1.01
2c	156.32 ± 1.42	170.25 ± 0.63	47.76 ± 1.45	37.68 ± 0.20
2d	163.68 ± 3.56	> 800	43.63 ± 3.20	74.36 ± 1.40
α-Tocopherol ^b	13.02 ± 5.17	19.92 ± 1.46	7.59 ± 0.53	31.52 ± 2.22

^a IC₅₀ values represent the means ± SEM of three parallel measurements ($p < 0.05$).

^b Reference compound.

compared to α-Tocopherol (31.52 ± 2.22 μM). The IC₅₀ value of compound **2c** was comparable to that of α-Tocopherol. The ABTS assay findings indicated that all tested pyrazolines derivatives possess significant antioxidant properties, with compound **2a** (10.48 ± 0.14 μM) demonstrating the highest antioxidant activity. The CUPRAC assay revealed that pyrazolines **2a** and **2b** exhibited antioxidant activity (A_{0.50} = 23.81 ± 0.25 and 35.21 ± 0.91 μM, respectively) comparable to α-Tocopherol (A_{0.50} = 19.92 ± 1.46 μM), while compound **2d** displayed significantly lower antioxidant activity (A_{0.50} > 800 μM).

From these results, compared to α-Tocopherol, it can be deduced:

- There is no correlation between the various antioxidant activities tests evaluated, which may be due to the different mechanisms of action employed by the assays.

- The synthesized pyrazoline derivatives exhibited significant antioxidant activity.
- Compound **2a** demonstrated higher antioxidant activity than the standard in the superoxide radical scavenging assay, and nearly equal antioxidant activity to the standard in the DPPH, ABTS, and CUPRAC assays. This could be attributed to the presence of two (—OH) groups at the ortho and para positions.

3.4. Evaluation of enzymatic inhibitory activity

The in vitro mushroom tyrosinase and acetylcholinesterase inhibitory activities of the synthesized compounds (**2a–2d**) were determined, and the results are presented in Table 4.

3.4.1. Evaluation of tyrosinase inhibitory activity

It is well known that the natural substrates tyrosine and L-DOPA contain phenolic hydroxyl, which is essential for tyrosinase inhibitory action. According to tyrosinase inhibitory results, compound **2a** exhibited the most potent anti-tyrosinase activity with an IC₅₀ of 32.65 ± 2.30 μM, almost equivalent to the standard kojic acid IC₅₀ = 25.23 ± 0.78 μM. This high anti-tyrosinase activity might be attributed to the presence of para and ortho-hydroxyl groups in their structure. Compounds **2b** and **2c** were less active than kojic acid by a factor of 2, while compound **2d** displayed 4-fold less potency compared to the reference used.

3.4.2. Evaluation of acetylcholinesterase inhibitory activity

Cholinesterase inhibitors provide a strategic approach for the treatment of neurodegenerative diseases such as Alzheimer's and Parkinson's. These inhibitors prevent the breakdown of choline, a crucial neurotransmitter associated with memory, by blocking the cholinesterase enzyme. Acetylcholinesterase (AChE) plays a key role in this process by breaking down acetylcholine into its components, choline, and acetic acid. This process is critical for resetting the cholinergic receptors in the body. Therefore, AChE has become a well-known target for treating Alzheimer's disease symptoms. By inhibiting AChE activity, acetylcholine levels in the brain can be increased, thereby improving cognitive function. The development of AChE inhibitors from natural resources may provide a safer alternative to synthetic drugs for treating Alzheimer's and other neurodegenerative diseases.

Compared to galantamine, a standard drug for Alzheimer's disease, compounds **2b–2d** displayed moderate anti-AChE activity (IC₅₀ = 21.65–59.65 μM). Pyrazoline **2a**, on the other hand, showed two times the potency of galantamine, with an IC₅₀ value of 3.93 ± 0.52 μM.

3.5. Target prediction

The top three targets—oxidoreductase (MAO-A, MAO-B) and hydrolase (ACHE)—and four tested compounds were assessed using SwissTargetPrediction. This tool is a web-based platform that predicts

Table 4

Tyrosinase and Acetylcholinesterase inhibitory activities of pyrazolines compounds.^a

Compounds	Tyrosinase inhibitory assay IC ₅₀ (μM) ^a	Anticholinesterase inhibitory assay IC ₅₀ (μM) ^a
2a	32.65 ± 2.30	3.93 ± 0.52
2b	54.68 ± 1.65	21.65 ± 1.96
2c	63.85 ± 1.70	30.35 ± 3.01
2d	106.56 ± 3.35	59.65 ± 2.54
Kojic acid ^b	25.23 ± 0.78	NT ^c
Galantamine ^b	NT ^c	6.27 ± 1.15

^a IC₅₀ values represent the means ± SEM of three parallel measurements ($p < 0.05$).

^b Reference compound.

^c Not tested.

the targets of small molecules based on a machine learning algorithm, using chemical and protein sequence similarity. It can predict the targets of over 3000 proteins from 1800 organisms. For testing using SwissTargetPrediction, the user can input a chemical structure or a SMILES string of the small molecule. The tool then analyzes the structure and generates a list of predicted targets along with a confidence score for each prediction. The predicted targets include proteins, enzymes, and receptors. SwissTargetPrediction can aid in drug discovery by identifying potential targets for a given small molecule, studying off-target drug effects, and predicting potential side effects. While it is freely available and widely used, it is crucial to validate predictions generated by SwissTargetPrediction experimentally before drawing conclusions. Here, the best receptor target probabilities for all four tested compounds were Monoamine oxidase B&A and Acetylcholinesterase. Monoamine oxidase B (MAO-B) and Monoamine oxidase A (MAO-A) are enzymes that play a crucial role in monoamine neurotransmitter metabolism, such as dopamine, serotonin, and norepinephrine. Compounds that selectively target MAO-B are more specific and have fewer off-target effects than those targeting both MAO-A and MAO-B. These compounds typically have a higher affinity for MAO-B and are used to treat neurodegenerative disorders like Parkinson's disease. MAO-B inhibitors like selegiline and rasagiline are commonly used to increase brain dopamine levels. Contrarily, compounds that target both MAO-A and MAO-B have broader therapeutic applications but may also have more side effects. These compounds are used to treat depression, anxiety, and other psychiatric disorders. MAO-A inhibitors, such as moclobemide and phenelzine, increase the levels of serotonin, norepinephrine, and dopamine in the brain. Compounds targeting MAO-B usually have a more selective mechanism of action, while those targeting both MAO-A and MAO-B have a broader range of therapeutic applications but may also have more side effects. The selectivity of a compound towards MAO-B or MAO-A can be determined by its chemical structure and binding affinity to the enzymes. It is also known that MAO-A and B are efficient targets for antidepressant drugs (Tables 5 and 6).

3.6. Drug-likeness studies

The drug-likeness of the synthesized pyrazolines was assessed according to Lipinski's Rule of Five, a set of criteria determining a molecule's drug-like qualities. These include a molecular weight less than 500 g/mol, no more than 10 hydrogen bond acceptors, no more than 5 hydrogen bond donors, a Log P value not exceeding 5, and a topological polar surface area (TPSA) less than 140 Å² [53]. The physicochemical and drug-like properties, assessed via SwissADME online servers, are shown in Table 7.

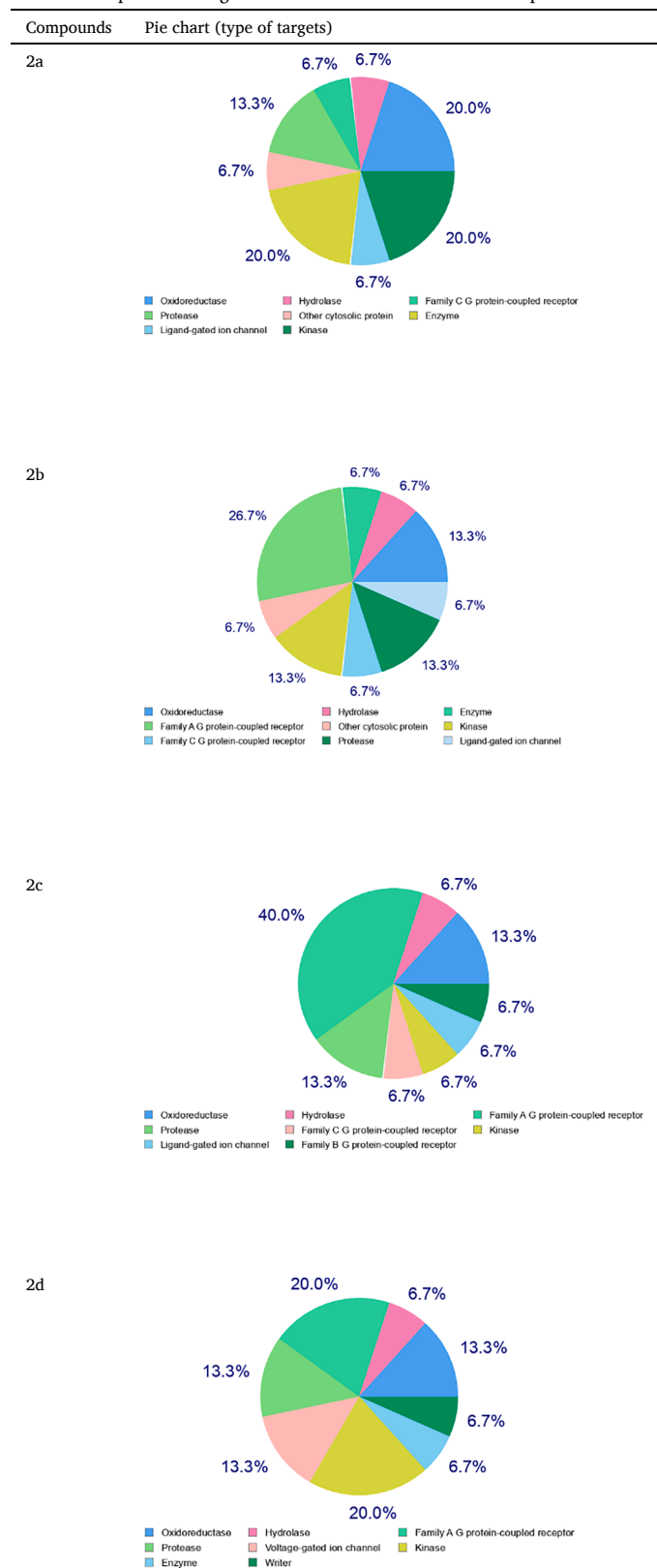
According to the Soft Drug-Like Rule, if a molecule exceeds two parameters, it may have poor absorption or permeability. Conversely, if only one parameter exceeds the limit, it is typically deemed acceptable [53]. With this rule and the data obtained, we conclude that compounds 2a and 2d meet Lipinski's criteria for drug-likeness with no violations. Compounds 2b and 2c exhibit one violation of Lipinski's classical criteria (MLOGP > 4.15), thus they may still be categorized as drug-like compounds.

Additionally, all synthesized pyrazolines align with the additional oral availability rules proposed by Veber. The estimated water solubility of the compounds studied is moderately soluble, with log S values ranging from -4.55 to -5.13 mg/mL. Furthermore, the consensus

Table 5
Potential Probability for each best 3 targets with all 4 tested compounds.

compound	MAO-A	MAO-B	ACHE
2a	0.509860935	0.576544658	0.509860935
2b	0.387931035	0.411675028	0.387931035
2c	0.553794489	0.553794489	0.285287513
2d	0.201584698	0.371181767	0.169270502

Table 6
Pie chart for potential targets classification for each tested compound.



model-calculated lipophilicity properties of the compounds, as measured by Log Po/w in n-octanol and water, were found suitable, ranging from 2.95 to 4.76 [54]. The prediction results suggest all tested pyrazoline derivatives exhibit high gastrointestinal (GI) absorption ($A >$

Table 7
ADMET parameters of the synthesized compounds.

Parameters	Compound 2a	Compound 2b	Compound 2c	Compound 2d
Physicochemical properties				
Formula	C ₁₉ H ₁₆ N ₂ O ₂	C ₁₉ H ₁₅ ClN ₂	C ₂₂ H ₂₂ N ₂	C ₂₀ H ₁₈ N ₂
Molecular weight (< 500 Da)	304.34 g/mol	306.79 g/mol	314.42 g/mol	286.37 g/mol
No. of heavy atoms	23	22	24	22
Fraction Csp3	0.11	0.11	0.23	0.15
No. of rotatable bonds	2	2	3	2
No. of H—bond acceptors ≤ 9	3	1	1	1
No. of H-bond donors ≤ 10	3	1	1	1
Molar Refractivity < 130	98.67	99.64	109.21	99.59
TPSA < 130	64.85 Å ²	24.39 Å ²	24.39 Å ²	24.39 Å ²
Lipophilicity				
LogP _{0/w} (iLOGP)	1.94	3.04	3.50	2.99
LogP _{0/w} (XLOGP3) < 5	3.87	5.20	5.70	4.94
LogP _{0/w} (WLOGP)	2.60	3.85	4.32	3.50
LogP _{0/w} (MLOGP)	2.59	4.28	4.45	4.01
LogP _{0/w} (SILICOS-IT)	3.74	5.36	5.82	5.25
Consensus LogP _{0/w}	2.95	4.35	4.76	4.14
Water Solubility				
Log S (ESOL)	−4.55	−5.42	−5.68	−5.13
Log S (Ali)	−4.93	−5.46	−5.98	−5.19
Log S (SILICOS-IT)	−6.11	−7.88	−8.08	−7.66
Drug-likeness				
Lipinski	Yes, 0 Violation	Yes; 1 violation: mLOGP > 4.15	Yes; 1 violation: mLOGP > 4.15	Yes, 0 Violation
Ghose	Yes	Yes	Yes	Yes
Veber	Yes	Yes	Yes	Yes
Egan	Yes	Yes	Yes	Yes
Muegge	Yes	No; 1 violation: XLOGP > 5	No; 1 violation: XLOGP > 5	Yes
Bioavailability Score	0.55	0.55	0.55	0.55
Pharmacokinetics				
Caco2	0.847	1.551	1.502	1.544
Intestinal adsorption human	88.887	90.913	91.917	92.371
Skin permeability	−2.777	−2.816	−2.845	−2.818
BBB permeability	0.096	0.426	0.528	0.476
CYP2D6 substrate	Yes	Yes	No	Yes
CYP3A4 substrate	Yes	Yes	Yes	Yes
CYP1A2 inhibitor	Yes	Yes	Yes	Yes
CYP2C19 inhibitor	Yes	Yes	Yes	Yes
CYP2C9 inhibitor	Yes	Yes	Yes	Yes
CYP2D6 inhibitor		No	Yes	No
CYP3A4 inhibitor	Yes	Yes	Yes	Yes
AMES toxicity	No	Yes	Yes	Yes
hERG I inhibitor	No	No	No	No
hERG II inhibitor	Yes	Yes	Yes	Yes
Hepatotoxicity	No	No	No	Yes
Skin Sensitisation	No	yes	No	No

30 %).

Skin permeability plays a crucial role in transdermal drug delivery and is a key factor in assessing product effectiveness. The studied compounds show low skin permeability, indicating potential use in alleviating skin allergies. The Caco-2 permeability values (log P_{app} > 0.90) for compounds **2b**, **2c**, and **2d** are predicted to be high. Compounds **2b**, **2c**, and **2d** may exhibit AMES toxicity, indicating possible mutagenic and carcinogenic effects. Moreover, compound **2b** may cause skin sensitization.

Inhibition of potassium channels, encoded by hERG (the human Ether-à-go-go-Related Gene), is known to cause long QT syndrome and fatal ventricular arrhythmia in hERG I and II inhibitors [55]. The obtained results reveal that all tested pyrazolines lack hERG I inhibitory properties while inhibiting hERG II.

The metabolism of small molecules depends heavily on the cytochrome (CYP) group of enzymes, which catalyze various oxidation processes and are responsible for biotransformation of approximately 90 % of marketed drugs [56,57]. Therefore, evaluating compounds' ability to inhibit cytochromes (CYP) is crucial for determining their metabolic activity. According to the obtained results, all tested compounds inhibit CYP1A2, CYP2C19, CYP2C9, and CYP3A4, except for compounds **2a** and **2c**. Compounds **2b** and **2d** were unable to inhibit the enzyme CYP2D6.

Additionally, based on the results, the bioavailability score of all tested compounds is 0.55, suggesting potential as effective oral medication. In summary, the synthesized pyrazoline derivatives are expected to exhibit a good pharmacokinetic profile and show promise as drugs, especially compound **2a**. Six physicochemical properties—flexibility, lipophilicity, thickness, polarity, solubility, and saturation—are depicted in the bioavailability radar (Fig. 7) obtained from the SwissADME website. These compound properties ideally fall within the pink region of the radar graph, indicating their drug-like properties. According to Fig. 7, all synthesized pyrazolines, except for saturation in **2a**, **2b**, and **2d**, lie within this pink region.

3.7. Gastrointestinal absorption and brain penetration prediction

Gastrointestinal absorption and brain access are two critical ADME properties assisting drug development prediction at various stages. The 'boiled egg' diagram is a proposed tool for accurate predictions [58]. When examining the boiled egg model of the pyrazoline molecules (Fig. 8), it appears that all tested compounds fall within the acceptable range. The diagram depicts blue dots (compounds **2a** and **2c**), representing molecules predicted to be excreted from the central nervous system by P-glycoprotein, and red dots (compounds **2b** and **2d**), and indicating molecules unlikely to be excreted. All compounds within the yellow zone suggest high gastrointestinal absorption and potential to cross the blood-brain barrier.

3.8. Molecular docking study

3.8.1. Docking against tyrosinase

To elucidate the mechanism of synthesized pyrazoline **2a** inhibition against mushroom tyrosinase and determine its favorable binding mode, a molecular docking study was performed. In silico docking results, including binding energy, best docked pose, and binding interactions of compound **2a** with mushroom tyrosinase, are shown in Table 8 and Fig. 9. For reliability, the co-crystallized kojic acid ligand was re-docked into the 2Y9X target.

Kojic acid (KA) is recognized for its potent anti-tyrosinase activity due to its ability to reduce o-dopaquinone back to L-Dopa and prevent melanin formation, aiding in skin hyperpigmentation treatment. The binding energy value of KA was −5.5 kcal/mol, forming three strong hydrogen bonds with the KA hydroxyl groups and key residues His61 (2.38 Å), His85 (3.05 Å), and Met280 (2.38 Å). The tested compound demonstrated a higher docking binding energy of −8.6 kcal/mol than KA. This difference is attributed to the molecular weight.

The literature indicates that His244, Glu256, Ala286, Asn260, Phe264, and Val283 are crucial residues in the tyrosinase enzyme's active center cavity [59,60]. Histidine residues (His61, His85, His94, His259, His263, and His296), which bind with binuclear copper, are also significant as they interact with inhibitors because they usually cannot interact directly with the copper ions key to the inhibitory effect. Compound **2a**, a strong in vitro tyrosinase inhibitor (IC₅₀ = 32.65 ± 2.30 μM), demonstrated good binding energy, involving three

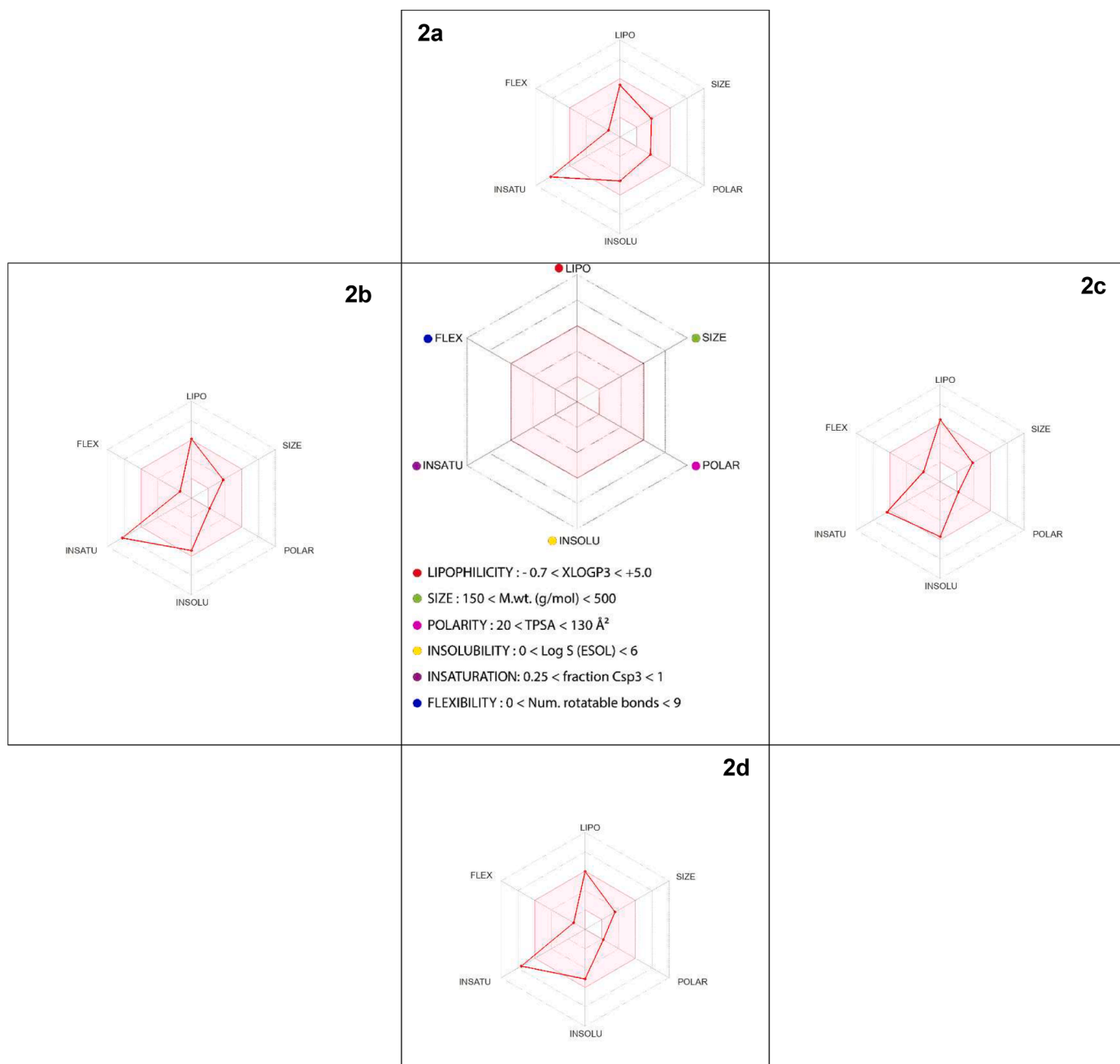


Fig. 7. Bioavailability radar of synthesized pyrazolines compounds.

conventional hydrogen bonds between the hydroxyl group H-atom, the N—H group H-atom, and the pyrazoline ring N-atom with Met280, Asn260, and His244 key residues, at intermolecular distances of 1.96 Å, 2.06 Å, and 2.29 Å, respectively. A π —Sigma interaction is observed between both aromatic rings and the 3-(naphthalen-2-yl) ring with Val248 and Val283, respectively. A carbon-hydrogen bond is also formed with His259. Interestingly, compound **2a** interacts with four key residues responsible for coordinating binuclear copper in the active site [61].

3.8.2. Docking against acetylcholinesterase

The binding interaction of the selected synthesized pyrazoline **2a** and galantamine against acetylcholinesterase (AChE) as a target enzyme was investigated using molecular docking. Table 8 and Fig. 10 depict the results of the tested compounds. Compound **2a** demonstrated promising performance against AChE compared to standard galantamine, with

docking scores of -11.6 and -9.2 kcal/mol, respectively, confirming experimental results. As indicated by the protein-ligand interaction (PLI) profiles (Fig. 10), compound **2a** exhibited key interactions with amino acid residues such as Ser286 (2.83 Å) and Arg289 (2.44 Å) through hydrogen bonding, Phe331 (3.58 Å) through carbon-hydrogen bonding, and Phe330 through π - π T-shaped bonding. It also forms π - π stacking interactions with Tyr334 and Trp279, and various amino acid interactions through van der Waals forces.

4. Conclusion

In this investigation, four novel pyrazoline derivatives, **2a**, **2b**, **2c**, and **2d**, were synthesized and their characteristics analyzed using spectroscopic methods. These derivatives were evaluated for their antioxidant capabilities as well as their inhibitory action against acetylcholinesterase (AChE) and Tyrosinase in vitro. The DFT/B3LYP

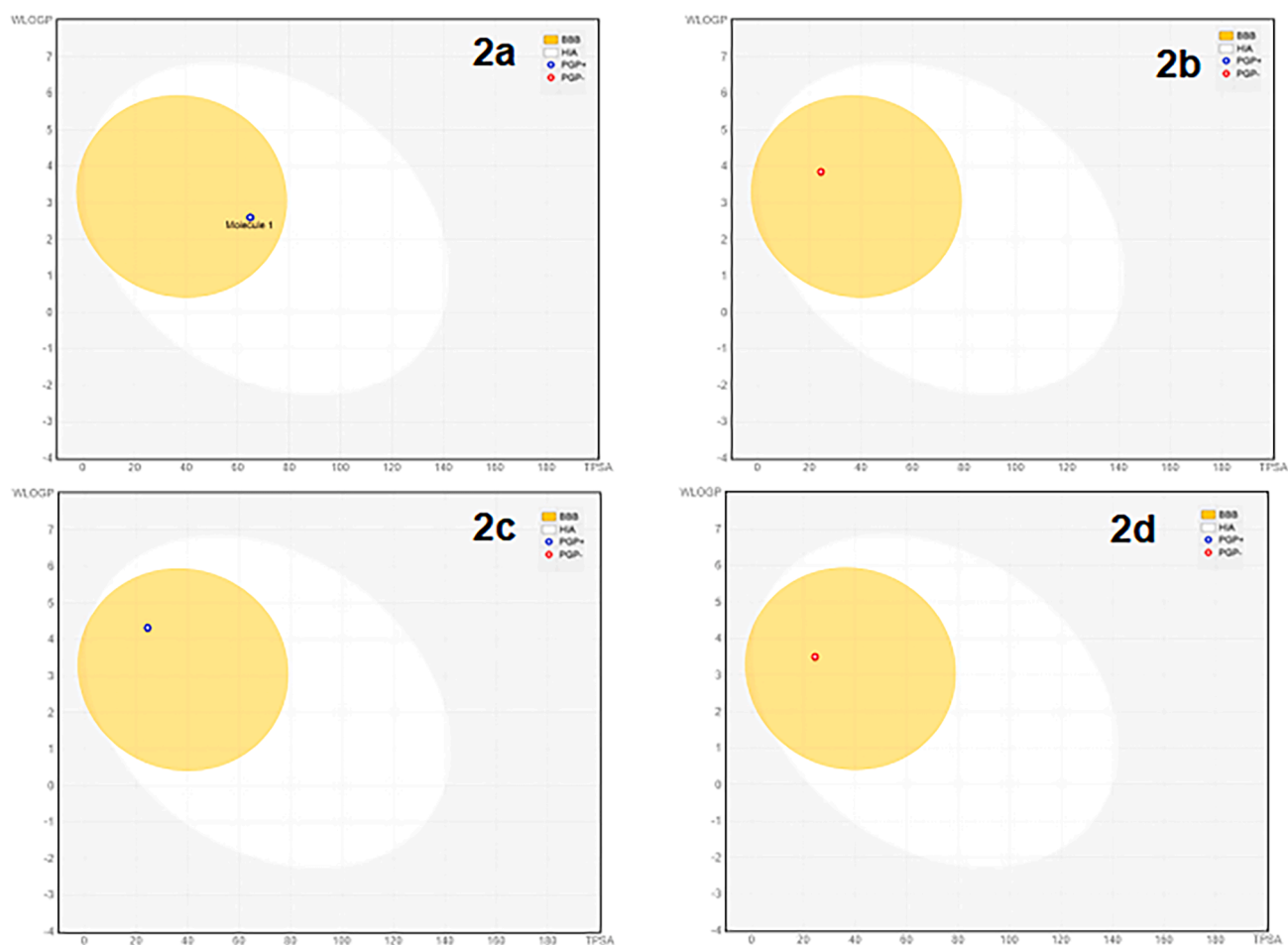


Fig. 8. The BOILED-Egg diagram of the pyrazoline compounds.

Table 8

Docking score, bond interactions-types and bond lengths of tyrosinase and AChE Protein (PDB ID: 2Y9X and 1ACL) with the selected compounds.

Target enzyme	Compound	receptor	Interaction type	Distance (Å°)	Docking score (Kcal/mol)	RMSD average (Å°)	
2Y9X	2a	His244	Conventional hydrogen bond	2.29	-8.6	3.5383	
		Asn260		2.09			
		Met280		1.96			
		Val248	π -sigma	3.70			
			Val283	π -sigma			3.78
			His259	Carbon hydrogen bond			3.51
	Kojic acid	His61	Conventional hydrogen bond	3.77			
		Met280		2.38			
		His85		2.57			
		Ala286	π -Alkyl	3.05			
His263		π - π stacked	4.97				
Val283		π -sigma	3.66				
1ACL	2a	Ser286	Conventional hydrogen bond	3.90	-11.6	3.2344	
		Arg289		2.83			
		Phe331	Carbon hydrogen bond	2.44			
		Tyr334	π - π stacked	3.58			
			Trp279				3.94
							3.92
			Phe330	π - π T-shaped			5.84
							4.59
							5.29
							4.95
Galantamine	Galantamine	Ser122	Conventional hydrogen bond	2.48	-9.2	2.0937	
		Gly118	Carbon hydrogen bond	3.33			
		His:440	π -alkyl	5.48			
		Tyr334	π -sigma	3.60			

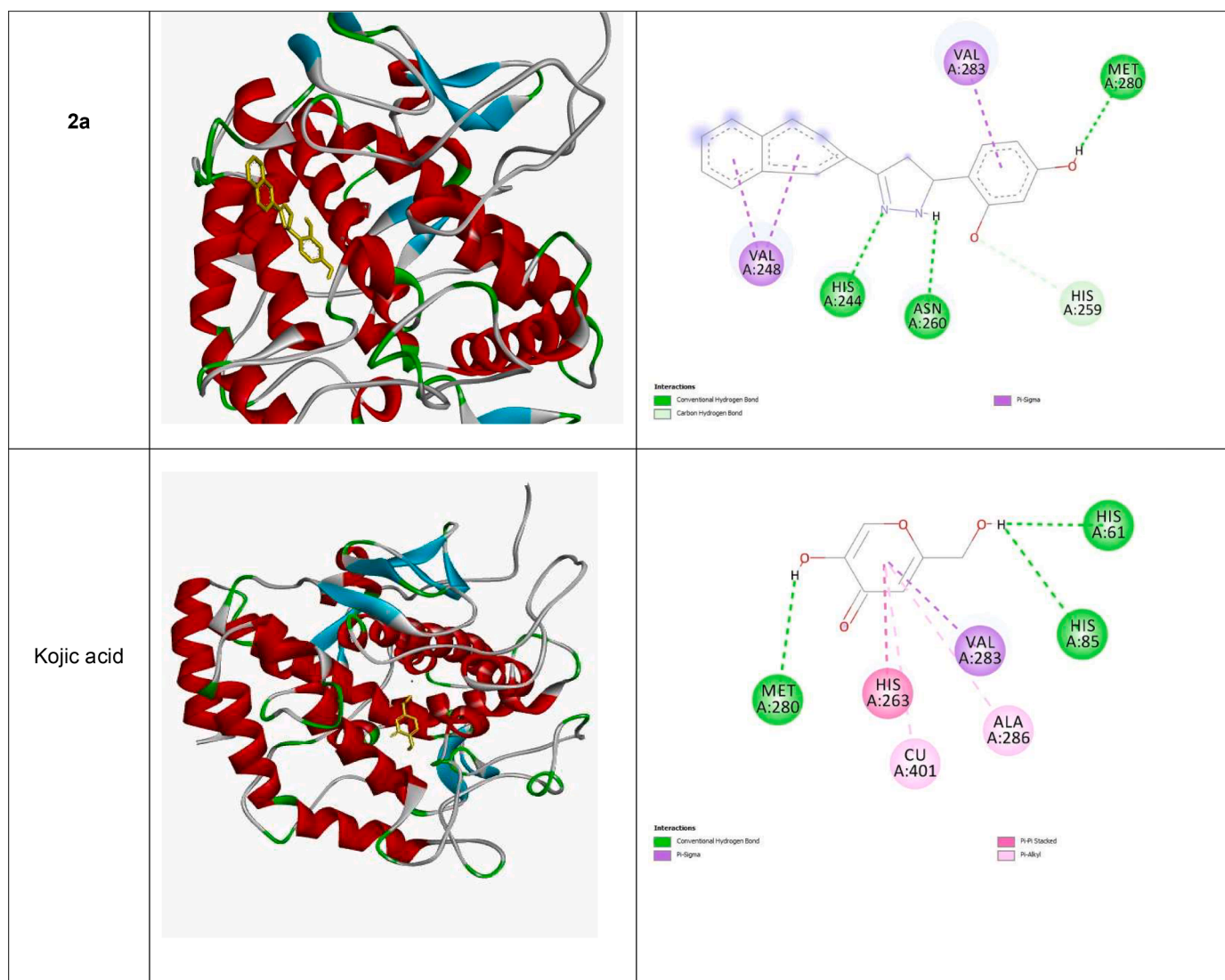


Fig. 9. Interactions of poses between compounds with the best binding affinity for tyrosinase (PDB:2Y9X).

quantum chemical computation method was applied to gain a deeper understanding of the molecular structure and reactivity of these compounds. The empirical results indicated that all of the tested compounds exhibited moderate to robust antioxidant activity. A screening for tyrosinase inhibitory potential revealed IC_{50} values that varied between 32.65 ± 2.30 and 106.56 ± 3.35 μ M. Compound **2a** stood out with a two-fold greater inhibitory effect against the AChE enzyme compared to the standard drug, with IC_{50} values of 3.93 ± 0.52 and 6.27 ± 1.15 μ M, respectively. The synthesized compounds **2a–2d** were also investigated for their potential as drug candidates through ADMET studies. The findings suggested that the synthesized pyrazoline derivatives could demonstrate promising pharmacokinetic profiles, making them potent drug candidates, particularly compound **2a**. Lastly, a molecular docking study was conducted to determine the binding affinity of the most active compound (**2a**), along with kojic acid and galantamine, with the AChE and tyrosinase enzymes. The results highlighted that the selected pyrazoline established several critical interactions, including conventional hydrogen bonding, carbon-hydrogen bonding, π – π T-shaped, π –alkyl, π – π stacking, and numerous van der Waals interactions, with the active sites of both AChE and tyrosinase enzymes. This finding indicates that the synthesized compounds, especially **2a**, have promising drug-like properties and might serve as effective inhibitors of AChE and tyrosinase enzymes.

CRediT authorship contribution statement

I. Selatnia: Supervision, Conceptualization, Methodology, Validation, Project administration, Writing – original draft, Writing – review & editing. **O.M.A. Khamaysa:** Formal analysis, Investigation, Writing – original draft. **A.G. Soliman:** Formal analysis, Investigation, Writing – original draft. **R. Bourzami:** Formal analysis, Investigation, Writing – original draft. **A. Sid:** Supervision, Conceptualization, Methodology, Validation, Project administration, Writing – original draft, Writing – review & editing. **H. Lgaz:** Supervision, Conceptualization, Methodology, Validation, Project administration, Writing – original draft, Writing – review & editing. **K. Mokhnache:** Investigation, Data curation, Writing – review & editing. **Awad A. Alrashdi:** Investigation, Data curation, Writing – review & editing. **C. Bensouici:** Investigation, Data curation, Writing – review & editing.

Declaration of Competing Interest

The authors declare that they have no known competing financial interests or personal relationships that could have appeared to influence the work reported in this paper.

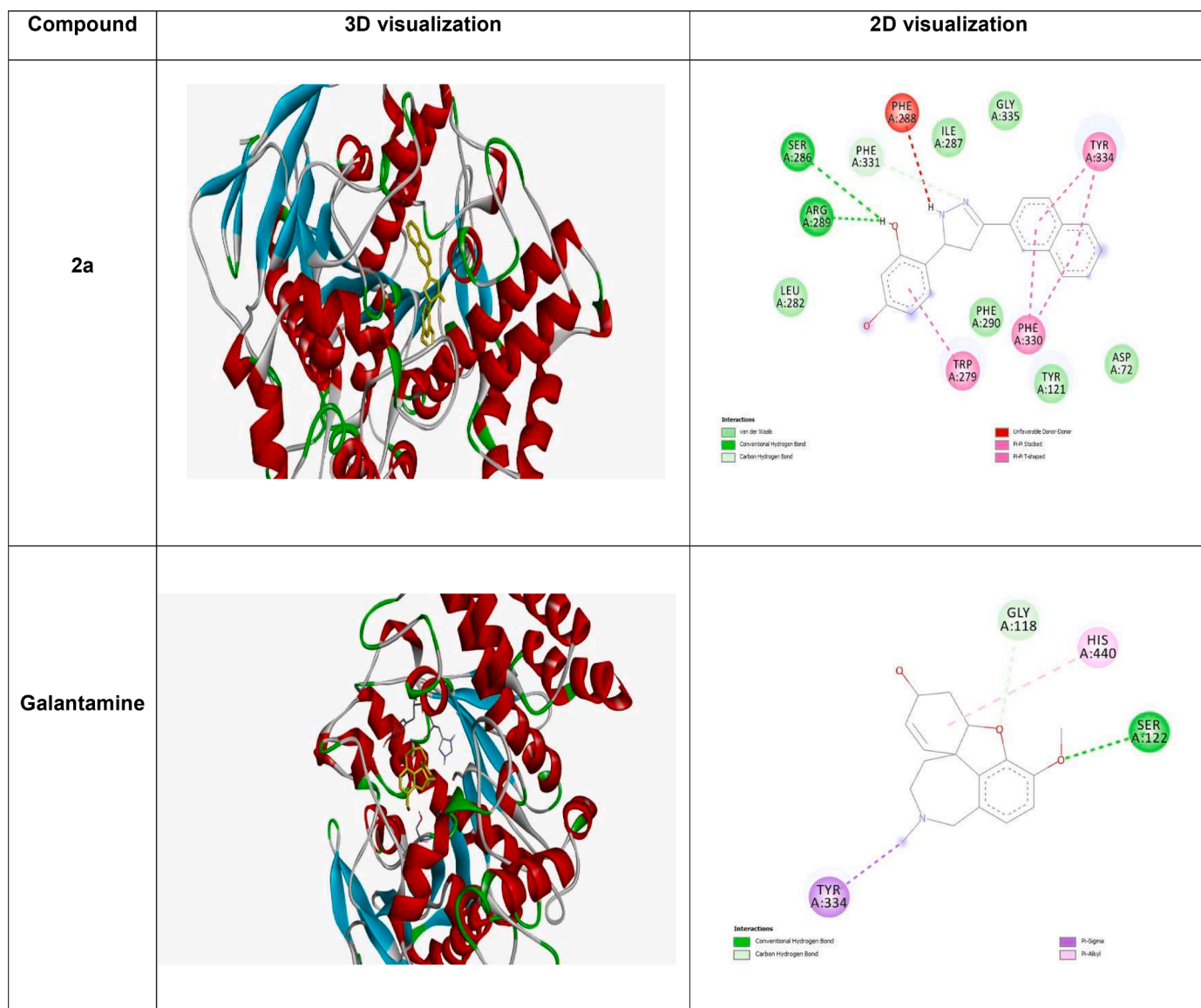


Fig. 10. Interactions of poses between compounds with the best binding affinity for Ache (PDB:1ACL).

Data availability

No data was used for the research described in the article.

Acknowledgment

The authors would like to thank the Algerian MESRS (Ministere de l'Enseignement Superieur et de la Recherche Scientifique) and DGRSDT (Direction Generale de la Recherche Scientifique et du Developpement Technologique).

“The authors would like to thank the Deanship of Scientific Research at Umm Al-Qura University for supporting this work by Grant Code: 23UQU4421201DSR02”

We gratefully acknowledge Mr. Paul Mosset Professor at the University of Rennes 1. France for providing spectroscopic analysis.

Supplementary materials

Supplementary material associated with this article can be found, in the online version, at [doi:10.1016/j.molstruc.2023.136761](https://doi.org/10.1016/j.molstruc.2023.136761).

References

- [1] A. Kumar, B.G. Varadaraj, R.K. Singla, Synthesis and evaluation of antioxidant activity of novel 3, 5-disubstituted-2-pyrazolines, *Bull. Faculty Pharm., Cairo Univ.* 51 (2) (2013) 167–173.
- [2] S. Hamadouche, A. Ounissi, K. Baira, N. Ouddai, M. Balsamo, A. Erto, Y. Benguerba, Theoretical evaluation of the antioxidant activity of some stilbenes using the Density Functional Theory, *J. Mol. Struct.* 1229 (2021), 129496.
- [3] H. Muğlu, B.Z. Kurt, F. Sönmez, E. Güzel, M.S. Çavuş, H. Yakan, Preparation, antioxidant activity, and theoretical studies on the relationship between antioxidant and electronic properties of bis (thio/carbohydrazone) derivatives, *J. Phys. Chem. Solids* 164 (2022), 110618.
- [4] M.D. Altintop, A. Özdemir, Z.A. Kaplancıklı, G. Turan-Zitouni, H.E. Temel, G. A. Çiftçi, Synthesis and biological evaluation of some pyrazoline derivatives bearing a dithiocarbamate moiety as new cholinesterase inhibitors, *Arch. Pharm. (Weinheim)* 346 (3) (2013) 189–199.
- [5] A.L. Hopkins, C.R. Groom, The druggable genome, *Nat. Rev. Drug Discovery* 1 (9) (2002) 727–730.
- [6] R.A. Copeland, *Evaluation of Enzyme Inhibitors in Drug Discovery: A Guide for Medicinal Chemists and Pharmacologists*, John Wiley & Sons, 2013.
- [7] H.E. Abdelwahab, H.Z. Ibrahim, A.Z. Omar, Design, synthesis, DFT, molecular docking, and biological evaluation of pyrazole derivatives as potent acetyl cholinesterase inhibitors, *J. Mol. Struct.* 1271 (2023), 134137.
- [8] C. Lynch, World Alzheimer Report 2019: attitudes to dementia, a global survey: public health: engaging people in AD/DR research, *Alzheimer's Dementia* 16 (2020), e038255.

- [9] A. Basiri, M. Xiao, A. McCarthy, D. Dutta, S.N. Byrareddy, M. Conda-Sheridan, Design and synthesis of new piperidone grafted acetylcholinesterase inhibitors, *Bioorg. Med. Chem. Lett.* 27 (2) (2017) 228–231.
- [10] A.M. Thawabteh, A. Jibreen, D. Karaman, A. Thawabteh, R. Karaman, Skin pigmentation types, causes and treatment—a review, *Molecules* 28 (12) (2023) 4839.
- [11] P. Goswami, H. Sharma, Skin hyperpigmentation disorders and use of herbal extracts: a review, *Curr. Trends Pharm. Res.* 7 (2) (2020) 81–104.
- [12] A. Korkmaz, E. Bursal, Synthesis, biological activity and molecular docking studies of novel sulfonate derivatives bearing salicylaldehyde, *Chem. Biodivers.* 19 (6) (2022), e202200140.
- [13] A. Korkmaz, E. Bursal, An in vitro and in silico study on the synthesis and characterization of novel bis (sulfonate) derivatives as tyrosinase and pancreatic lipase inhibitors, *J. Mol. Struct.* 1259 (2022), 132734.
- [14] A. Korkmaz, G. Kurtay, E. Kaya, E. Bursal, Design, synthesis, spectroscopic characterizations, in vitro pancreatic lipase as well as tyrosinase inhibition evaluations and in silico analysis of novel aryl sulfonate-naphthalene hybrids, *J. Biomol. Struct. Dyn.* 41 (15) (2023) 7128–7143.
- [15] A. Korkmaz, E. Bursal, Benzothiazole sulfonate derivatives bearing azomethine: synthesis, characterization, enzyme inhibition, and molecular docking study, *J. Mol. Struct.* 1257 (2022), 132641.
- [16] K. Singh, R. Pal, S.A. Khan, B. Kumar, M.J. Akhtar, Insights into the structure activity relationship of Nitrogen-containing heterocyclics for the development of antidepressant compounds: an updated review, *J. Mol. Struct.* (2021), 130369.
- [17] Z. Ye, F. Zhang, Recent advances in constructing nitrogen-containing heterocycles via electrochemical dehydrogenation, *Chin. J. Chem.* 37 (5) (2019) 513–528.
- [18] M. Henary, C. Kananda, L. Rotolo, B. Savino, E.A. Owens, G. Cravotto, Benefits and applications of microwave-assisted synthesis of nitrogen containing heterocycles in medicinal chemistry, *RSC Adv.* 10 (24) (2020) 14170–14197.
- [19] D. Jabli, M.L. Efrif, STRUCTURAL CHARACTERIZATION, DFT and an efficient synthetic route towards novel 1-phosphonate (5-amino-4-cyano-pyrazol-1-yl) phosphonic derivatives by the ternary condensation of alpha-ethyl cyanocinnamate and (thio) diethyl phosphorylhydrazides, Moroccan J. Heterocyc. Chem. 21 (01) (2022) 48–67, 21-01 (2022).
- [20] I. Kostopoulou, A. Diassakou, E. Kavetsou, E. Kritsi, P. Zoumpoulakis, E. Pontiki, D. Hadjipavlou-Litina, A. Detsi, Novel quinolinone-pyrazoline hybrids: synthesis and evaluation of antioxidant and lipoxigenase inhibitory activity, *Mol. Divers.* 25 (2021) 723–740.
- [21] V. Monga, K. Goyal, M. Steindel, M. Malhotra, D.P. Rajani, S.D. Rajani, Synthesis and evaluation of new chalcones, derived pyrazoline and cyclohexenone derivatives as potent antimicrobial, antitubercular and antileishmanial agents, *Med. Chem. Res.* 23 (4) (2014) 2019–2032.
- [22] P.M. Sivakumar, S. Ganesan, P. Veluchamy, M. Doble, Novel chalcones and 1, 3, 5-triphenyl-2-pyrazoline derivatives as antibacterial agents, *Chem. Biol. Drug Des.* 76 (5) (2010) 407–411.
- [23] N.P. Rai, V.K. Narayanaswamy, S. Shashikanth, P.N. Arunachalam, Synthesis, characterization and antibacterial activity of 2-[1-(5-chloro-2-methoxy-phenyl)-5-methyl-1H-pyrazol-4-yl]-5-(substituted-phenyl)-[1, 3, 4] oxadiazoles, *J. Med. Chem.* 44 (11) (2009) 4522–4527.
- [24] S.Y. Hassan, Synthesis, antibacterial and antifungal activity of some new pyrazoline and pyrazole derivatives, *Molecules* 18 (3) (2013) 2683–2711.
- [25] Z.A. Kaplancikli, A. Özdemir, G. Turan-Zitouni, M.D. Altıntop, Ö.D. Can, New pyrazoline derivatives and their antidepressant activity, *J. Med. Chem.* 45 (9) (2010) 4383–4387.
- [26] B. Nehra, S. Rulhania, S. Jaswal, B. Kumar, G. Singh, V. Monga, Recent advancements in the development of bioactive pyrazoline derivatives, *J. Med. Chem.* 205 (2020), 112666.
- [27] M.D. Altıntop, Synthesis, in vitro and in silico evaluation of a series of pyrazolines as new anticholinesterase agents, *Lett. Drug Des. Discov.* 17 (5) (2020) 574–584.
- [28] M.J. Ahsan, A. Ali, A. Ali, A. Thiriveedhi, M.A. Bakht, M. Yusuf, O. Afzal Salahuddin, A.S.A. Altamimi, Pyrazoline containing compounds as therapeutic targets for neurodegenerative disorders, *ACS Omega* 7 (43) (2022) 38207–38245.
- [29] R. Aggarwal, A. Bansal, I. Rozas, B. Kelly, P. Kaushik, D. Kaushik, Synthesis, biological evaluation and molecular modeling study of 5-trifluoromethyl-Δ2-pyrazoline and isomeric 5/3-trifluoromethylpyrazole derivatives as anti-inflammatory agents, *J. Med. Chem.* 70 (2013) 350–357.
- [30] D.K. Achutha, C.B. Vagish, N. Renuka, D.M. Lokeshwari, A.K. Kariyappa, Green synthesis of novel pyrazoline carbothioamides: a potent antimicrobial and antioxidant agents, *Chem. Data Collect.* 28 (2020), 100445.
- [31] K.N. Venugopala, M. Habeebuddin, B.E. Aldhubiab, A.H. Asif, Design, synthesis, and in vitro evaluation of novel indolyl dihydropyrazole derivatives as potential anticancer agents, *Molecules* 26 (17) (2021) 5235.
- [32] M. Rana, R. Arif, F.I. Khan, V. Maurya, R. Singh, M.I. Faizan, S. Yasmeen, S.H. Dar, R. Alam, A. Sahu, Pyrazoline analogs as potential anticancer agents and their apoptosis, molecular docking, MD simulation, DNA binding and antioxidant studies, *Bioorg. Chem.* 108 (2021), 104665.
- [33] N. Kahriman, Z. Haşimoğlu, V. Serdaroğlu, F.Ş. Beriş, B. Barut, N. Yaylı, Synthesis of novel pyrazolines, their boron–fluorine complexes, and investigation of antibacterial, antioxidant, and enzyme inhibition activities, *Arch. Pharm. (Weinheim)* 350 (2) (2017), 1600285.
- [34] S.R. Kazmi, R. Jun, M.-S. Yu, C. Jung, D. Na, In silico approaches and tools for the prediction of drug metabolism and fate: a review, *Comput. Biol. Med.* 106 (2019) 54–64.
- [35] X. Yu, X. Cai, S. Li, L. Luo, J. Wang, M. Wang, L. Zeng, Studies on the interactions of theaflavin-3, 3'-digallate with bovine serum albumin: multi-spectroscopic analysis and molecular docking, *Food Chem.* 366 (2022), 130422.
- [36] F. Javaheri-Ghezeldizaj, M. Mahmoudpour, R. Yekta, J.E.N. Dolatabadi, Albumin binding study to sodium lactate food additive using spectroscopic and molecular docking approaches, *J. Mol. Liq.* 310 (2020), 113259.
- [37] A. Sid, K. Lamara, M. Mokhtari, N. Ziani, P. Mosset, Synthesis and characterization of 1-formyl-3-phenyl-5-aryl-2-pyrazolines, *Eur. J. Chem.* 2 (3) (2011) 311–313.
- [38] A. Sid, F. Mahdi, A. Messai, N. Ziani, M. Mokhtari, Synthesis, characterization and antimicrobial screening of some novel 3-(naphthalen-1 and 2-yl)-5-aryl-2-pyrazolines synthesized by condensation of hydrate hydrazine to appropriate α, β-unsaturated ketones, *J. Chem., Biol. Phys. Sci.* 5 (2) (2015) 1125–1130.
- [39] A.D. Becke, Density-functional exchange-energy approximation with correct asymptotic behavior, *Phys. Rev. A* 38 (6) (1988) 3098.
- [40] T. Tsuneda, J.-W. Song, S. Suzuki, K. Hirao, On Koopmans' theorem in density functional theory, *J. Chem. Phys.* 133 (17) (2010), 174101.
- [41] R.G. Parr, R.G. Pearson, Absolute hardness: companion parameter to absolute electronegativity, *J. Am. Chem. Soc.* 105 (26) (1983) 7512–7516.
- [42] R.G. Parr, R.A. Donnelly, M. Levy, W.E. Palke, Electronegativity: the density functional viewpoint, *J. Chem. Phys.* 68 (8) (1978) 3801–3807.
- [43] M.S. Blois, Antioxidant determinations by the use of a stable free radical, *Nature* 181 (4617) (1958) 1199.
- [44] R. Apak, K. Güçlü, M. Özyürek, S.E. Karademir, Novel total antioxidant capacity index for dietary polyphenols and vitamins C and E, using their cupric ion reducing capability in the presence of neocuproine: CUPRAC method, *J. Agric. Food Chem.* 52 (26) (2004) 7970–7981.
- [45] R. Re, N. Pellegrini, A. Proteggente, A. Pannala, M. Yang, C. Rice-Evans, Antioxidant activity applying an improved ABTS radical cation decolorization assay, *Free Radical Biol. Med.* 26 (9–10) (1999) 1231–1237.
- [46] E. Kunchandy, M. Rao, Oxygen radical scavenging activity of curcumin, *Int. J. S8* (3) (1990) 237–240.
- [47] G.L. Ellman, K.D. Courtney, V. Andres Jr, R.M. Featherstone, A new and rapid colorimetric determination of acetylcholinesterase activity, *Biochem. Pharmacol.* 7 (2) (1961) 88–95.
- [48] E. Chan, Y. Lim, L. Wong, F. Lianto, S. Wong, K. Lim, C. Joe, T. Lim, Antioxidant and tyrosinase inhibition properties of leaves and rhizomes of ginger species, *Food Chem.* 109 (3) (2008) 477–483.
- [49] O.A. Chaves, T.P. Calheiro, J.C. Netto-Ferreira, M.C. de Oliveira, S.Z. Franceschini, C.M.C. de Salles, N. Zanatta, C.P. Frizzo, B.A. Iglesias, H.G. Bonacorso, Biological assays of BF2-naphthyridine compounds: tyrosinase and acetylcholinesterase activity, CT-DNA and HSA binding property evaluations, *Int. J. Biol. Macromol.* 160 (2020) 1114–1129.
- [50] H. Dong, J. Liu, X. Liu, Y. Yu, S. Cao, Combining molecular docking and QSAR studies for modeling the anti-tyrosinase activity of aromatic heterocycle thiosemicarbazone analogues, *J. Mol. Struct.* 1151 (2018) 353–365.
- [51] I. Selatnia, A. Sid, M. Benahmed, T. Ozturk, N. Gherraf, Synthesis and characterization of a bis-pyrazoline derivative as corrosion inhibitor for A283 carbon steel in 1 M HCl: electrochemical, surface, DFT and MD simulation studies, *Protect. Metals Phys. Chem. Surfaces* 54 (6) (2018) 1182–1193.
- [52] E.E. Ebeson, D.A. Isabirye, N.O. Eddy, Adsorption and quantum chemical studies on the inhibition potentials of some thiosemicarbazides for the corrosion of mild steel in acidic medium, *Int. J. 11* (6) (2010) 2473–2498.
- [53] S. Ejeh, A. Uzairu, G.A. Shallangwa, S.E. Abechi, M.T. Ibrahim, Structure-based design, drug-likeness, and pharmacokinetic studies of novel substituted pyrimidine derivatives as potent HCV NS3/A4 protease inhibitors, *Biocatal. Agric. Biotechnol.* 46 (2022), 102539.
- [54] A. Mermer, S. Alyar, Synthesis, characterization, DFT calculation, antioxidant activity, ADMET and molecular docking of thiosemicarbazide derivatives and their Cu (II) complexes, *Chem. Biol. Interact.* 351 (2022), 109742.
- [55] T. Yeşilkaynak, F.N. Özkömeç, M. Çeşme, R.E. Demirdöğen, C.V. Sezer, H.M. Kutlu, F.M. Emen, Novel thiourea derivative compounds: thermal behavior, biological evaluation, Hirshfeld surfaces and frontier orbitals analyses, in silico ADMET profiling and molecular docking studies, *J. Mol. Struct.* 1280 (2023), 135086.
- [56] M. Ibrahim, A. Uzairu, 2D-QSAR, molecular docking, drug-likeness, and ADMET/pharmacokinetic predictions of some non-small cell lung cancer therapeutic agents, *J. Taibah Univ. Med. Sci.* 18 (2) (2023) 295.
- [57] U.M. Zanger, M. Schwab, Cytochrome P450 enzymes in drug metabolism: regulation of gene expression, enzyme activities, and impact of genetic variation, *Pharmacol. Ther.* 138 (1) (2013) 103–141.
- [58] A. Daina, V. Zoete, A boiled-egg to predict gastrointestinal absorption and brain penetration of small molecules, *ChemMedChem* 11 (11) (2016) 1117–1121.
- [59] Q. Yu, L. Fan, Z. Ding, The inhibition mechanisms between asparagus polyphenols after hydrothermal treatment and tyrosinase: a circular dichroism spectrum, fluorescence, and molecular docking study, *Food Biosci.* (2022), 101790.
- [60] Y.-X. Si, S. Ji, W. Wang, N.-Y. Fang, Q.-X. Jin, Y.-D. Park, G.-Y. Qian, J. Lee, H.-Y. Han, S.-J. Yin, Effects of boldine on tyrosinase: inhibition kinetics and computational simulation, *Process Biochem.* 48 (1) (2013) 152–161.
- [61] M. Miastkowska, P. Śliwa, Influence of terpene type on the release from an O/W nanoemulsion: experimental and theoretical studies, *Molecules* 25 (12) (2020) 2747.